Chapter 6

A review of the Chemical Index of Alteration (CIA) and its application to the study of Neoproterozoic glacial deposits and climate transitions

HEINRICH BAHLBURG[1]* & NICOLE DOBRZINSKI[2]

[1]*Institut für Geologie und Paläontologie, Westfälische Wilhelms-Universität, 48149 Münster, Germany*

[2]*RWE Dea AG, Wietze Laboratory, 29323 Wietze, Germany*

**Corresponding author (e-mail: hbahlburg@uni-muenster.de)*

Abstract: The Chemical Index of Alteration (CIA) is the most accepted of available weathering indices. Past conditions of physical and chemical weathering can be reliably inferred if application of the CIA is combined with a comprehensive facies analysis. When applied to the reconstruction of climate conditions during Neoproterozoic times, CIA data provide crucial insights into the changes in the relative contributions of chemical and physical weathering in the production of sedimentary detritus. CIA data are thus instrumental not only in documenting changes between icehouse and greenhouse climates, but also in recognizing shorter-term climate oscillations between glacial and warm–humid conditions. Concerning the Neoproterozoic glacial periods, sedimentological and CIA data sets give strong evidence of a functioning hydrological cycle, operative sediment routing systems, and variable climate conditions oscillating between dry–cool and glacial, and warm–humid and interglacial. These findings are incompatible with the hypothesis of a totally ice-covered Snowball Earth.

Climate exerts the major control on weathering processes affecting the upper continental crust. Direct evidence of past weathering conditions and thus climate can be obtained from palaeosols through a combination of, among other things, field observation, petrography (particularly diagenetic phases), X-ray diffractometry and whole rock and isotope geochemistry. However, palaeosols are restricted to continental environments, which commonly have a relatively low preservation potential. Even though palaeosoils as old as Palaeoproterozoic are reported in the literature (e.g. Gutzmer & Beukes 1998; Nedachi *et al.* 2005), most information on weathering conditions and thus climate has to be gleaned from reworked siliciclastic material deposited in marine or lacustrine environments. In the Precambrian eon, which represents nearly 90% of Earth history, marine siliciclastic sedimentary rocks are the most widely available source of information on past climates.

In Phanerozoic rocks, information derived from siliciclastic sedimentary rocks may be supplemented by ecological indicators derived from fossils. However, the bearing of palaeofaunal data on the interpretations of palaeoclimate conditions needs to be considered very carefully, because differences between continental regimes of weathering and marine environments of deposition may be very large. This is illustrated for example by the pronounced difference at the coast of northern Chile between conditions of extreme subtropical aridity in the Atacama desert and the cold waters of the Humboldt current originating in the peri-Antarctic westwind drift.

Extreme climate states are of particular interest to palaeoclimate research. Among these, those that figure most prominently are the icehouse climates that happened in at least five cycles of highly variable duration and extent during Earth history, that is, the Palaeoproterozoic and Neoproterozoic, Ordovician, Carboniferous–Permian and Neogene glaciations (Crowley & North 1991; Crowell 1999). Of these, the Neoproterozoic glaciations are some of the most discussed and contentious (e.g. Hoffman *et al.* 1998; Evans 2000; Hoffman & Schrag 2002; Eyles & Januszczak 2007; Fairchild & Kennedy 2007; Etienne *et al.* 2008; Eyles 2008). The timing and causes of the inception and termination of Neoproterozoic glacial states as well as variations in the severity of the icehouse conditions themselves remain unresolved issues (e.g. Schrag *et al.* 2002; Baum & Crowley 2003; Fairchild & Kennedy 2007; Shields 2008).

Unfortunately, in many cases, facies analysis of sedimentary rocks does not supply unambiguous information on palaeoclimate conditions. This conundrum is well illustrated by the mutually exclusive interpretations of the Neoproterozoic, that is, Marinoan, Ghaub Formation diamictites (Otavi Group) in northern Namibia. These have been interpreted either as glaciogenic sediments (Gevers 1931; Martin 1964; Hoffmann & Prave 1996; Hoffman & Schrag 2002) or as tectonically triggered mass flow deposits (Schermerhorn 1974; Martin *et al.* 1985; Eyles & Januszczak 2007). However, these issues may be moved closer to resolution through a combination of facies analysis with considerations of weathering as a function of climate (e.g. Young & Nesbitt 1999; Young 2001; Scheffler *et al.* 2003).

In this contribution we will review the most important weathering proxies applied to siliciclastic sedimentary rocks. We will concentrate on the CIA (Nesbitt & Young 1982) and its potential and limitations for deriving palaeoclimate information from glacial and pre- and post-glacial siliciclastic successions. We will preferentially but not exclusively address Neoproterozoic glacial successions based on a combination of published information from the Nanhuan–Sinian glacial succession in South China (Dobrzinski *et al.* 2004; Dobrzinski & Bahlburg 2007) and new data on the Port Askaig Formation (Scotland), the Ghaub Formation (northern Namibia) and the Mortensnes and Smalfjord formations (northern Norway).

Weathering and weathering indices

Exposed rocks are affected to variable degrees by a combination of chemical and physical weathering (Bland & Rolls 1998). Progressive chemical weathering of labile minerals like feldspar leads to the loss of Ca^{2+}, K^{+} and Na^{+} and the transformation to minerals more stable under surface conditions (Fedo *et al.* 1995). Ultimately, it results in the formation of shales rich in clay minerals such as illite and kaolinite, and Fe-oxyhydrates such as goethite. Physical weathering, in turn, leads to the degradation of rocks to smaller grain sizes, ideally without causing geochemical and

From: Arnaud, E., Halverson, G. P. & Shields-Zhou, G. (eds) *The Geological Record of Neoproterozoic Glaciations*. Geological Society, London, Memoirs, **36**, 81–92. 0435-4052/11/$15.00 DOI: 10.1144/M36.6

mineralogical changes. If physical weathering, and the grinding action of moving ice-lodged debris in particular, degrades a source rock into a clay-sized deposit, it should essentially preserve the mineralogical and geochemical composition of the original rock (Nesbitt & Young 1982, 1996). Consequently, the character of the climate framework and the way it governs weathering conditions and reactions is reflected by the mineralogical and mobile element geochemical composition of the resulting deposits, and the shales and clay-sized materials in particular.

Ultimately, chemical weathering of silicate rocks leads through hydrolysis to an exchange of the cations Na^+, K^+, Ca^{2+} and Mg^{2+} for H^+, and maybe a loss of Si^{4+} (Kramer 1968). Na^+, K^+ and Ca^{2+} are commonly supplied by the weathering of feldspar and volcanic glass, together accounting for *c.* 58% of the exposed crust. Mg^{2+} is derived from glasses, sheet silicates and mafic minerals and resides in chloritic and smectitic clays (Nesbitt & Young 1984; Pettijohn *et al.* 1987). In general, hydrolytic weathering causes a progressive transformation of affected components into clay minerals, ultimately kaolinite. In a qualitative way, mineralogical changes can be detected in shales and sandstones using X-ray diffractometry. Optical analysis is a quantitative option in sandstones only. Here, the Mineralogical Index of Alteration (MIA), given by the ratio of quartz to the sum of quartz + K-feldspar + plagioclase, permits an assessment of weathering effects (Johnsson 1993). Quantitative estimations of weathering in fine-grained as well as coarse-grained rocks are relatively easily achieved by using whole-rock geochemical data to calculate geochemical weathering proxies. A comprehensive review of a great number of geochemical weathering indices has been presented by Duzgoren-Aydin *et al.* (2002).

Recently, von Eynatten *et al.* (2003) and von Eynatten (2004) presented a quantitative approach, the *t*-index, to statistically model linear compositional and weathering trends. If corroborated by further studies the *t*-index will likely lead to more quantitative definitions of weathering trends. A related statistical approach has been taken by Ohta & Arai (2007), whose *W* index is based on principal component analysis of eight major oxides. As yet, it has been applied only to igneous rocks.

Geochemical estimations of weathering effects need to be considered carefully, because the major cations Na^+, K^+ and Ca^{2+} may also be mobile under diagenetic conditions (Wintsch & Kvale 1994). Geochemical weathering proxies make use of the changes of bulk-rock geochemical composition caused by chemical alteration. A very simple proxy is the Ruxton Ratio *R* (Ruxton 1968) given by the SiO_2/Al_2O_3 ratio. This assumes that Al_2O_3 remains immobile during weathering, and changes in *R* therefore reflect silica loss as a proxy for total element loss. The Ruxton Ratio may be useful when weathering profiles on rocks of felsic and intermediate composition are considered, but was found to be poorly correlated to the actual weathering grade of a silicate rock (Duzgoren-Aydin *et al.* 2002).

As the transformation of feldspar to clay minerals and the coincident mobility of the main cations is a major process of chemical (i.e. hydrolytical) weathering, Parker (1970) considered it more useful to mirror changes in Na^+, K^+, Ca^{2+} and Mg^{2+} and created a weathering index (WIP, Weathering Index of Parker) given by

$$\mathrm{WIP} = \left(\frac{\mathrm{Na}^*}{0}.35 + \frac{\mathrm{Mg}^*}{0}.9 + \frac{\mathrm{K}^*}{0}.25 + \frac{\mathrm{Ca}^*}{0}.7\right) \times 100 \quad (1)$$

where the cations* represent the atomic percentage of an element divided by the atomic weight. Parker (1970) also considered the susceptibility of these elements to weathering by including in the denominator Nicholls' values of bond strength as a measure of the energy necessary to break the cation-to-oxygen bonds of the respective oxides. These different values are considered to reflect the probability of an element being mobilized during the weathering process. Values of WIP are commonly between $\geq$100 and 0, with the least weathered rocks having the highest values (Fig. 6.1). The WIP implicitly assumes that all Ca^{2+} in a silicate rock is contained in silicate minerals. This simplification is a source of imprecision of the index, particularly if larger amounts of carbonate detritus or cements are present in the rock. More problematic still is the lack of consideration of a relatively immobile reference phase like Al_2O_3 in the formula, which would help to monitor relative changes of composition of the relevant mineral components.

The disadvantages of the WIP are overcome in the Chemical Index of Alteration (CIA) using whole-rock geochemical data of major element oxides (Nesbitt & Young 1982). The index is essentially based on the same considerations that led Kramer (1968) to

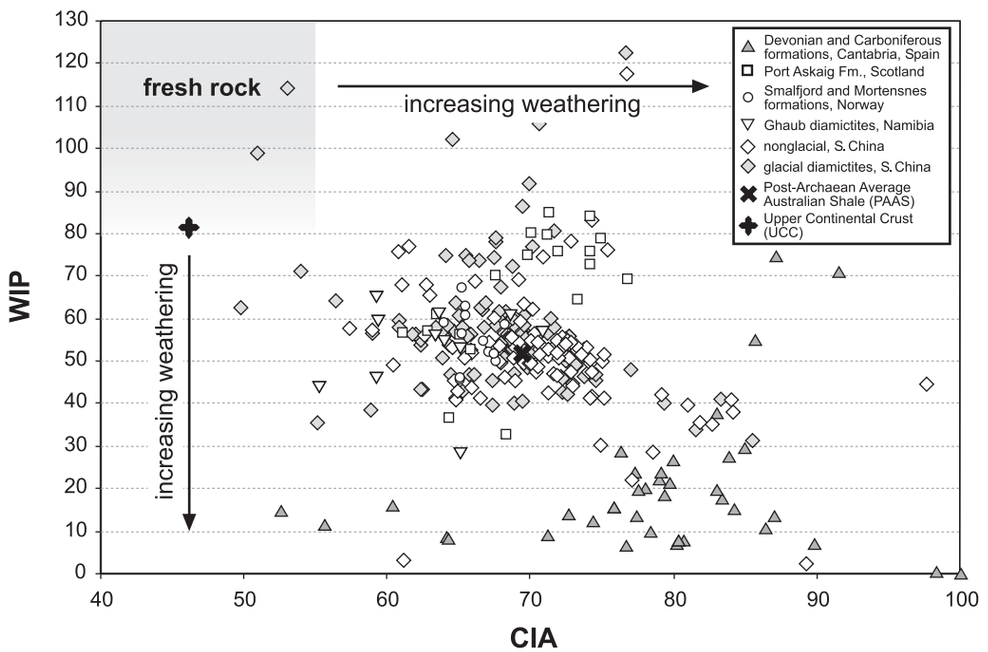

Fig. 6.1. Relationship between two weathering proxies, WIP (Parker 1970) and CIA (Nesbitt & Young 1982). Shown are data obtained from the matrix of Neoproterozoic glacial diamictites from South China (Dobrzinski *et al.* 2004), the Port Askaig Formation, Scotland (Panahi & Young 1997, and this study, Table 6.3), the Ghaub Formation of northern Namibia (Table 6.4), and the Smalfjord and Mortensnes formations, northern Norway (Table 6.4). Also shown are data from non-glacial shales and siltstones including those underlying, intercalated with and overlying the South China glacial diamictites, and well-weathered Palaeozoic shales from the Cantabrian mountain belt of Hercynian age in northern Spain (Table 6.1).

Table 6.1. *Sampled formations and compositional groupings discussed in this contribution*

Lithostratigraphic units, terminology, this paper	Formation	Region	Rock types	Sampled lithology	Depositional age	Ref.
Devonian and Carboniferous formations, Cantabria	Vergaño, Vañes, Carmen, Potes Group, Murcia	Northern Spain	Quartz sandstone, sandstone, siltstone, shale	Shale, siltstone	Late Devonian to Carboniferous	Wagner & Wagner-Gentis (1963), IGME (1984), ITGE (1994), Keller *et al.* (2008)
Mortensnes and Smalfjord formations	Mortensnes, Smalfjord	Northern Norway	Diamictite, shale	Siltstone, shale	Ediacaran, Neoproterozoic	Rice & Hoffmann (2001), Arnaud & Eyles (2002), Rice *et al.* (2011)
Port Askaig Formation	Port Askaig	Scotland	Diamictite	Diamictite matrix: shale, siltstone	Cryogenian, Neoproterozoic	Panahi & Young (1997), Arnaud & Eyles (2006), Benn & Prave (2006), Arnaud & Fairchild (2011)
Ghaub diamictites, Namibia	Ghaub	Otavi Mountains, northern Namibia	Diamictite, siltstone	Silicate shale matrix, siltstone	Cryogenian, Neoproterozoic	Hoffman & Schrag (2002), Eyles (2007), Hoffman (2011)
Non-glacial, South China (post-glacial)	Doushantuo, Jinjiadong	Yangtze platform, South China	Carbonate, shale	Shale	Ediacaran, Neoproterozoic	Dobrzinski *et al.* (2004), Dobrzinski & Bahlburg (2007), Zhang *et al.* (2011)
Glacial, South China, (upper diamictites)	Nantuo, Hongjiang, Leigongwu	Yangtze platform, South China	Diamictite	Diamictite matrix: shale, siltstone	Cryogenian, Neoproterozoic	Dobrzinski *et al.* (2004), Dobrzinski & Bahlburg (2007), Zhang *et al.* (2011)
Non-glacial, South China (inter-glacial)	Datanpo, Xianmeng, Lantian	Yangtze platform, South China	Carbonate, shale	Shale	Cryogenian, Neoproterozoic	Dobrzinski *et al.* (2004), Dobrzinski & Bahlburg (2007), Zhang *et al.* (2011)
Glacial, South China, (lower diamictites)	Dongshanfeng, Jiangkou, Tie-si-ao	Yangtze platform, South China	Diamictite	Diamictite matrix: shale, siltstone	Cryogenian, Neoproterozoic	Dobrzinski *et al.* (2004), Dobrzinski & Bahlburg (2007), Zhang *et al.* (2011)
Non-glacial, South China (pre-glacial)	Xieshuihe, Wuqiangxi, Zitang	Yangtze platform, South China	Sandstone, shale	Shale	Tonian and Cryogenian, Neoproterozoic	Dobrzinski *et al.* (2004), Dobrzinski & Bahlburg (2007), Zhang *et al.* (2011)

conclude that monitoring the hydrolysis of feldspar and volcanic glass and the respective changes in the content of the major cations offers the best quantitative measure of chemical weathering. It represents a ratio of predominantly immobile Al_2O_3 to the mobile cations Na^+, K^+ and Ca^{2+} given as oxides. The CIA is defined as

$$\mathrm{CIA} = \left(\frac{\mathrm{Al_2O_3}}{\mathrm{Al_2O_3} + \mathrm{Na_2O} + \mathrm{K_2O} + \mathrm{CaO^*}}\right) \times 100 \qquad (2)$$

where the major element oxides are given in molecular proportions. CaO* represents the CaO content of silicate minerals only (Fedo *et al.* 1995) and thus eliminates one of the disadvantages of the WIP. Kaolinite has a CIA value of 100 and represents the highest degree of weathering. Illite is between 75 and *c.* 90, muscovite is at 75, and the feldspars at 50. Fresh basalts have values between 30 and 45, fresh granites and granodiorites between 45 and 55 (Nesbitt & Young 1982; Fedo *et al.* 1995; Fig. 6.1).

Careful attention has to be paid to the potential presence of clastic carbonate grains or of carbonate cement in the sedimentary rock. If undetected but abundant, both would lead to very low and unrealistic CIA values. The presence of carbonate grains or cements (calcite or dolomite) and the ratio of calcite to dolomite have to be determined petrographically. Both can be effectively accounted for geochemically by determining total MgO and CaO and the total inorganic carbon (TIC) content of a sample, all of which can then be used to calculate relative contributions to CO_2, and finally CaO* (Fedo *et al.* 1995; Tables 6.2, 6.3, 6.4). Ca in phosphates may not be considered in calculation of the CIA, because CIA values will increase by not more than *c.* 1 unit if all P_2O_5 present in common siliciclastic rocks is assigned to apatite.

The CIA has been successfully applied in a large number of studies involving glacial deposits (e.g. Young & Nesbitt 1999; Young 2001; Condie *et al.* 2001; Scheffler *et al.* 2003; Dobrzinski *et al.* 2004; Young *et al.* 2004; Rieu *et al.* 2007) and other depositional environments (e.g. Gallet *et al.* 1998; Aristizábal *et al.* 2005; Kahmann *et al.* 2008).

A brief discussion of WIP and CIA

Results of a comparison of WIP and CIA are displayed in Fig. 6.1. It combines data on Neoproterozoic glaciomarine deposits from South China (Dobrzinski *et al.* 2004) and the Port Askaig Formation (Scotland; Panahi & Young 1997; and our own analyses) with new data on the Ghaub Formation (Namibia) and the Mortensnes and Smalfjord formations of northern Norway (Tables 6.1 to 6.4). For comparison we also show hitherto unpublished results on a number of late Devonian and early Carboniferous siliciclastic shales and siltstones from the Palentinian foreland basin (Keller *et al.* 2007, 2008) of the Hercynian Cantabrian Mountain belt in northern Spain (Table 6.1). In the Late Palaeozoic, the Palentinian Basin was located at near-equatorial latitudes (Weil *et al.* 2001). We use the Cantabrian data as an example of well-weathered detritus developed under non-glacial conditions.

The WIP values of the glacial Ghaub, Port Askaig, Mortensnes and Smalfjord formations fall between 29 and 107, with a majority between 40 and 80 (averages: Ghaub, 76; Mortensnes and

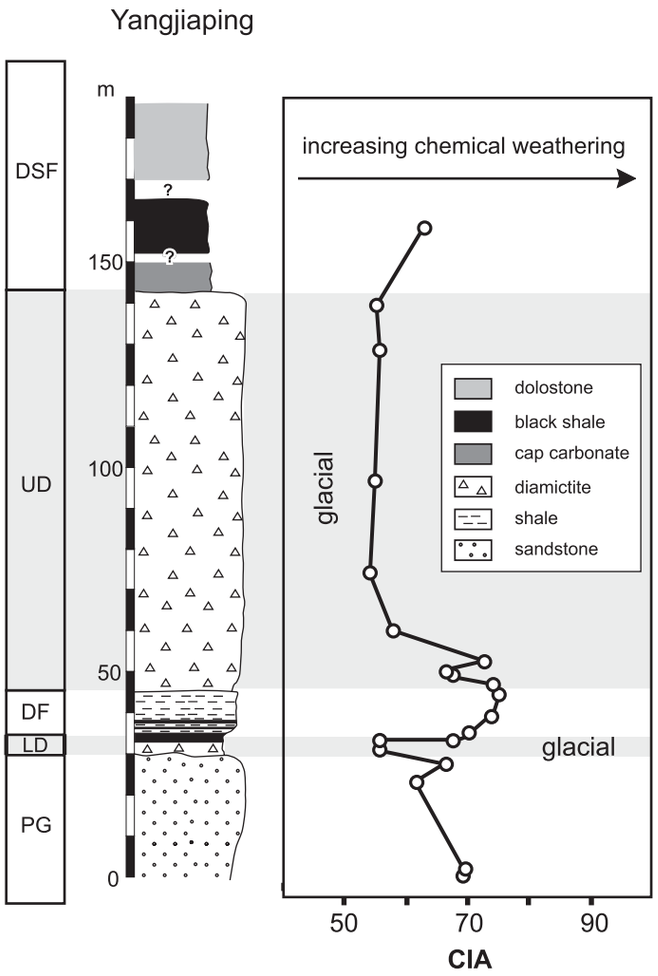

Fig. 6.2. The Yangjiaping section in South China and its Neoproterozoic climate record indicated by CIA values. PG, preglacial units; LD, lower diamictite; DF, Datangpo Formation; UD, upper diamictite; DSF, Doushantuo Formation (Table 6.1). Note the initially high CIA values in the lower part of the upper diamictite unit followed by a decrease interpreted as the initial and then waning incorporation of chemically weathered detritus into the glacial deposit. *Source:* modified from Dobrzinski *et al.* (2004).

Smalfjord, 56; Port Askaig, 66; Fig. 6.1). In contrast, the Cantabrian formations demonstrate their well-weathered character with values between 0 and 75, with a majority below 40 (average, 19). Considering these formations, the WIP appears to differentiate well between glacial and non-glacial weathering types.

The CIA values of the glacial units fall within 55 and 77 with a majority below 70 (averages: Ghaub, 63; Mortensnes and Smalfjord, 66; Port Askaig, 70; Fig. 6.1). These are typical values of unweathered to slightly weathered detritus and conform well to a glacial weathering regime. The Cantabrian shales and siltstones, in turn, reflect the dominance of warm–humid weathering conditions with a CIA between 56 and 100 and an average of 79.

The glacial and non-glacial deposits from South China seem to complicate the picture because they both have relatively low as well as high WIP values typical of intense and weak chemical weathering, respectively (Fig. 6.1). The WIP range of the glacial deposits is 31–121 with an average of 57. The respective values of the non-glacial formations are 2–118 and 52. CIA values are distributed between 50 and 85 in the glacial deposits (average, 68) and between 55 and 85 with the rare sample having a value of close to 100 (average, 71; Fig. 6.1; Dobrzinski *et al.* 2004).

The values of both indices seem to demonstrate that both the glacial and non-glacial Neoproterozoic sedimentary rocks in South China consist of a mixture of detritus of glacial and non-glacial weathering provenance, albeit in different proportions. The initial incorporation of weathered older detritus into the Neoproterozoic glacial deposits was demonstrated by Dobrzinski *et al.* (2004) by upward trends to lower CIA values in several sections in South China (Fig. 6.2). Similar observations were made by Panahi & Young (1997) in the Port Askaig Formation, Scotland.

K-feldspar and plagioclase are relatively common in the Chinese glacial and non-glacial deposits. The presence of labile feldspar indicates that the non-glacial rocks did not form predominantly under humid and warm–humid conditions. Regarding the weathering sensitive cations K^+ and Na^+, average values for Na_2O in both the glacial and non-glacial deposits from South China are 1.3 wt%, whereas the average value of detritus derived from the upper continental crust is 1.2 wt% (PAAS, Post-Archaean average Australian shale, Taylor & McLennan 1985). Condie (1993) gives an estimate of Na_2O in the average Proterozoic shale (APS) derived from the Proterozoic upper crust of 1.1 wt%.

Average K_2O values of 3.3 wt% coincide with the Proterozoic upper crust, upper continental crust and Average Proterozoic shale values of 3.3, 3.4 and 3.6 wt%, respectively (Condie 1993; McLennan 2001). Considering the calculations of the respective indices, an increase in, for example, Na_2O of 0.5 wt% causes a decrease in the CIA of *c.* 2.5 units, and an increase of WIP of 5 units. A decrease by 0.5 wt% results in similar, but opposing, changes in magnitude. In the case of K_2O the effect is similar; however, the change in CIA units is *c.*1.5 per 0.5 wt% change. The respective changes in WIP are *c.* $\pm$ 4 units.

Our data demonstrate that both the WIP and CIA appear to be equally sensitive to small changes in the concentrations of the major cations, and thus, by inference, of dominant warm–humid or dry–cold weathering conditions. Disadvantages of the WIP include the lack of consideration of mobile relative to immobile phases, and the fact that it is based on whole-rock CaO and not on CaO* of the silicate fraction only. Another advantage of the CIA lies in the way it permits the definition and prediction of weathering trends of silicate rocks (Nesbitt & Young 1982, 1984). Data and trends can then be displayed well in A–CN–K (Al_2O_3 – CaO* + Na_2O – K_2O) ternary diagrams (Fig. 6.3; Nesbitt & Young 1984). The combination of these features makes the CIA the presently preferred weathering index.

Provenance and reconstruction of original compositions

Provenance pathways and the distribution of lithologies in source regions exert a first-order control on the composition of siliciclastic deposits (Johnsson 1993). Differences in provenance are therefore reflected also in the weathering indices (Fedo *et al.* 1995). In the ternary A–CN–K diagram of Figure 6.3, the provenance compositions and weathering trends can be depicted and predicted. Hydrolytic weathering leads to a loss of Na^+ and Ca^{2+} and changes rock compositions towards the A apex and ever higher CIA values.

Transport sorting exerts another major influence on the composition of clastic sediments. Along a river and transport path, labile mineral grains will be comminuted preferentially. In the presence of chemical weathering, labile grains like feldspar will be prone to progressive decay along cleavages, cracks and other zones of lattice weakness. Feldspars will eventually be transformed into clay minerals and a marked compositional difference, in addition to the comminution of mineral grains, between source and sediment will become evident (Johnsson *et al.* 1988). Sorting will thus lead to a higher proportion of clay minerals downriver and consequently higher CIA values (Nesbitt *et al.* 1997; Fig. 6.3). Thus, when CIA values of different successions are compared, similar grain sizes need to be considered.

Only exceptional circumstances permit the transfer of labile mineral grains from source to sink without any mineralogical

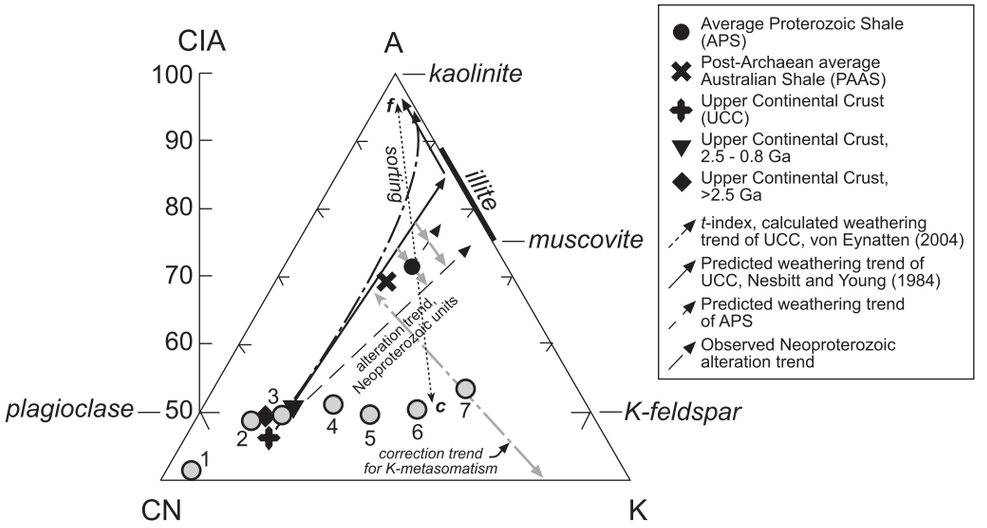

Fig. 6.3. Major oxides in molecular ratios with compositions of typical magmatic source rock types (Fedo *et al.* 1995) and average compositions of the UCC through time (UCC, McLennan 2001; PAAS, Taylor & McLennan 1985; all others, Condie 1993). Note that the lower part of the diagram with A < 40 is not shown. 1, gabbro; 2, tonalite; 3, granodiorite; 4, granite; 5, A-type granite; 6, charnokite; 7, potassic granite. Ideal weathering trends of UCC-type source lithologies would be parallel to the predicted weathering trend (Nesbitt & Young 1984). The statistically modelled *t*-index weathering trend (von Eynatten 2004) is based on data obtained from the world's major rivers and erosional products of major denudation areas (McLennan 1993). Trends of K-metasomatism and its graphical correction to pre-metasomatic values on predicted weathering trends is indicated by grey arrows originating or pointing at the K apex of the diagram (Fedo *et al.* 1995). Alteration trend of Neoproterozoic glacial successions estimated from the distribution of samples in Fig. 6.4. The dotted double-headed arrow outlines the effect of grain sorting on the chemical composition of sediments and consequently on CIA values; *c*, coarse, sand; *f*, fine, clay (Nesbitt *et al.* 1997).

and thus compositional changes, that is, without the influence of any chemical weathering. In such an ideal case transport will lead only to comminution of mineral grains; the final fine-grained deposit will have the same composition as the coarser source (Nesbitt & Young 1996), and CIA values will be unaffected.

Diagenetic addition of potassium to a deposit during illitization of kaolinite and the replacement of plagioclase or illite by K-feldspar, the so called K-metasomatic effect of Fedo *et al.* (1995), causes weathered compositions to plot closer to the K apex (Fig. 6.3), thus resulting in diagenetically lowered CIA values. This can be checked by comparisons with average upper crustal compositions (see above) and by comparing CIA values with K/Cs ratios (McLennan *et al.* 1993); a K-metasomatic effect would disturb the pronounced negative correlation between the K/Cs ratio and weathering intensity. The distribution of data in the A–CN–K diagram (Fig. 6.4) indicates that in particular some of the Chinese sedimentary rocks discussed in this paper show a weak K-metasomatic effect (Dobrzinski *et al.* 2004). If projected back to the predicted weathering trend originating from average granodiorite or the upper continental crust (UCC) (Fig. 6.3), the originally higher CIA values of these samples can be reconstructed (Tables 6.3 and 6.4), thus permitting the subsequent inference of original provenance compositions (Figs 6.3 and 6.4; Fedo *et al.* 1995).

As the CIA is founded essentially in considerations of the mobility of the major cations, geochemical estimations of provenance

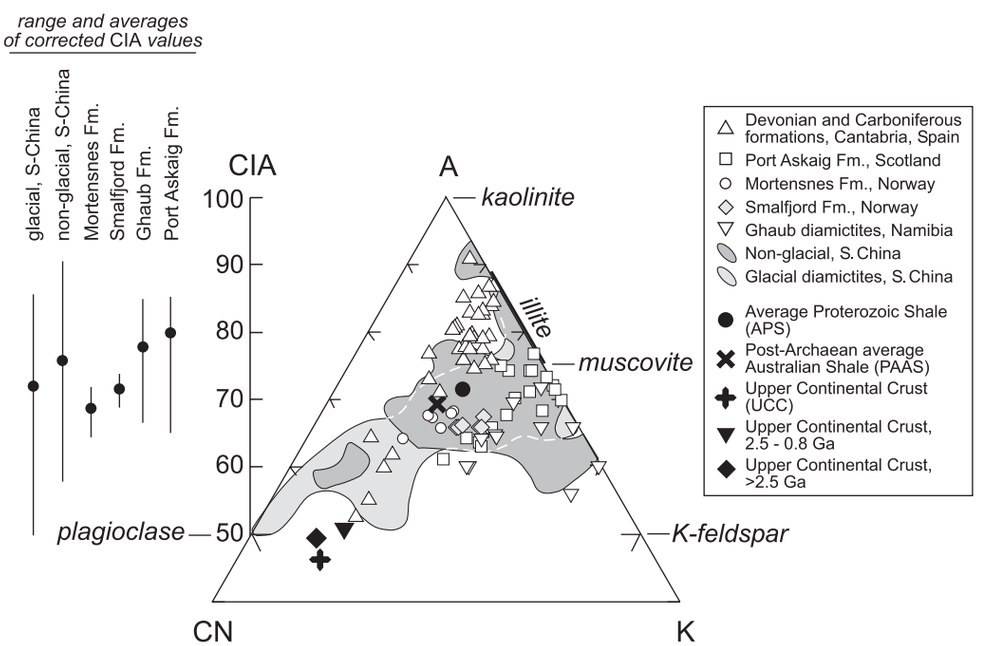

Fig. 6.4. A–CN–K (Al_2O_3–CaO*+Na_2O–K_2O) diagram with data of Neoproterozoic glacial units and reference units and their composition (PAAS, Taylor & McLennan 1985; UCC, McLennan 2001; all others, Condie 1993). Note that the lower part of the diagram with A < 40 is not shown. The left side of the figure shows the range and averages (black dots) of CIA values of the Neoproterozoic units corrected for K-metasomatism according to Fedo *et al.* (1995). For comparison, the figure also shows data obtained from shales of several late Devonian and Carboniferous formations from the Palentinian foreland basin of the Hercynian Cantabrian mountain belt in northern Spain (Keller *et al.* 2008), which conform to the predicted weathering trend (Tables 6.1, 6.2; Nesbitt & Young 1984).

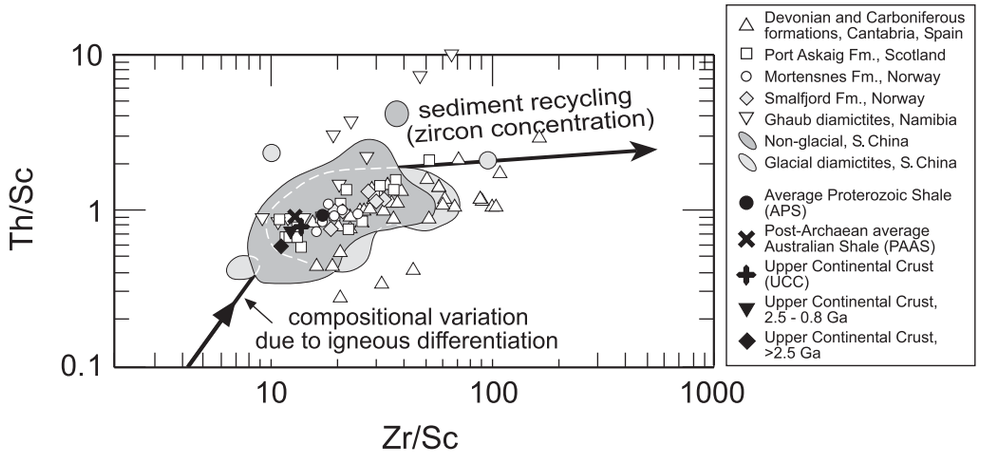

Fig. 6.5. Zr/Sc v. Th/Sc diagram of McLennan *et al.* (1993) demonstrating that all studied sedimentary rocks have an upper crustal composition and were affected to minor degrees by recycling, which is indicated by high Zr/Sc values. This effect is most prominently shown in some of the Late Palaeozoic sedimentary rocks from Cantabria. It is noteworthy that all the Neoproterozoic samples cluster around the composition of the average Proterozoic shale (APS, Condie 1993). Reference units and their composition: PAAS, Taylor & McLennan (1985); UCC, McLennan (2001); all others, Condie (1993).

should be combined preferably with ratios of immobile elements including the high field strength elements La, Th, Sc and Zr (Bhatia & Crook 1986; McLennan *et al.* 1993; Bahlburg 1998). All the Neoproterozoic sedimentary rocks considered in this paper have Zr/Sc and Th/Sc ratios similar to or higher than the Upper Continental Crust (UCC) and PAAS (Fig. 6.5; Taylor & McLennan 1985; McLennan 2001). The rock compositions all cluster around the composition of the APS (Fig. 6.5; Condie 1993) as a proxy for material derived from the average Proterozoic upper crust. This provides another indication that processes beyond original weathering and recycling did not significantly alter the composition of the studied Neoproterozoic sedimentary rocks.

Weathering trends

Thermodynamic, kinetic, experimental and observational evidence define weathering trends for silicate rocks that are (sub)parallel to the CN–A join of the A–CN–K diagram (Nesbitt & Young 1982, 1984). Weathering of average granodiorite or UCC along the predicted weathering trend (Fig. 6.3) will result in the transformation of labile components including the feldspars first to illite, thus causing the sample's composition to plot ever closer to the A–K join and the illite composition in A–CN–K space (Nesbitt & Young 1984; Fig. 6.3). Increasing formation of kaolinite during progressive weathering will curve the weathering trend towards the A apex when approaching the A–K join (Nesbitt & Young 1984) in a way similar to the calculated weathering trend of von Eynatten *et al.* (2004; Fig. 6.3). The validity of this general weathering behaviour and trend is substantiated by the fact that the compositions of shale composites like PAAS and APS as averaged samples of the weathered and recycled upper crust plot very near the predicted weathering trend (Fig. 6.3). Also, the Late Palaeozoic reference samples from Cantabria, Spain, which were well weathered under non-glacial conditions, plot along this trend as predicted by CIA systematics (Figs 6.3 & 6.4; Nesbitt & Young 1982, 1984).

In many cases, sedimentary rocks do not plot on the predicted weathering trend but below it, thus reflecting an increase in K^+ in the samples (e.g. Panahi & Young 1997; Rieu *et al.* 2007). A correction of this K-metasomatic effect according to Fedo *et al.* (1995) of those CIA data points below the predicted weathering trend line results in an increase of CIA values (Figs 6.3, 6.4; Tables 6.3, 6.4). This increase depends on the compositional difference between the sample and the predicted original value and reflects the degree of K-metasomatism having affected a sample's detritus if the original composition was granodioritic and close to that of the UCC (Fig. 6.3; Fedo *et al.* 1995). If the original composition was richer in K^+ than granodiorite or UCC, the predicted weathering trend would shift to the right but remain (sub)parallel to the predicted weathering trend (Nesbitt & Young 1984). Corrections for K-metasomatism and resulting increases in CIA values would be correspondingly smaller. A correction to the predicted weathering trend thus represents a maximum correction if average granodiorite or UCC is the starting point.

The average compositions of post Archaean shale and Proterozoic shale (PAAS, Taylor & McLennan 1985; APS, Condie 1993) plot below the predicted weathering trend towards the K apex of the A–CN–K diagram. This may be due either to starting compositions richer in K^+ than UCC and the average Proterozoic upper crust (Fig. 6.3), or a mild K-metasomatic effect including the conversion under increased temperature of illite to secondary K-feldspar (Nesbitt & Young 1989; Fedo *et al.* 1995).

The composition of almost all considered Neoproterozoic units and samples appears to systematically deviate from the predicted weathering trend, in a way here preliminarily called the observed Neoproterozoic alteration trend (Fig. 6.3). In discussing this trend, two things have to be borne in mind: the similarity of the estimates for the UCC and the average Proterozoic crust in A–CN–K space, and the fact that glaciogenic deposits commonly represent averaged samples of the available upper crust exposed to denudation.

It is a reasonable assumption that the original average geochemical composition of the silicate sources feeding the Neoproterozoic glaciogenic deposits was similar to the average upper crustal compositions. Repeated weathering and recycling processes may lead to a stepwise increase of K^+ in the resulting deposits, as indicated by the offsets of the average shale compositions from the predicted weathering trend (Fig. 6.3). The observed Neoproterozoic alteration trend may consequently reflect the degree to which unweathered and weathered crust and recycled sedimentary rocks have been mixed and incorporated into the glaciogenic deposits. The correction of CIA values for a K-metasomatic effect according to Fedo *et al.* (1995) will thus reconstitute CIA values to the predicted weathering trend originating in fresh upper crust, which may, however, be unrepresentative of the actually eroded continental surface. If CIA values were referred back only to unweathered compositions, irrespective of the regional context and the recycling history, estimates of weathering effects during the last sedimentary cycle will be exaggerated and may consequently be misleading.

The evidence of glaciomarine deposits

Successions of modern and ancient glacial deposits and of glacially derived detritus are ideally characterized by low CIA values reflecting the dominance of physical over chemical weathering processes (Nesbitt & Young 1982; Young 2001). A typical example is the Palaeoproterozoic Gowganda Formation (Young

Table 6.2. *Major element whole-rock compositions and weathering indices of shales*

Sample*	SiO_2	Al_2O_3	Fe_2O_3	MgO	CaO‡	Na_2O	K_2O	TiO_2	P_2O_5	MnO	LOI	Total	TC	TIC	WIP	CIA†
BT Nr.64	96.83	1.85	0.60	0.04	–	–	–	0.23	0.08	0.01	0.42	100.06			0	100
MB 87-K	95.33	2.40	0.61	0.02	–	–	0.04	0.23	0.04	0.01	0.72	99.41			0	98
MB P-05	87.40	3.54	0.83	0.12	2.49	0.07	0.41	0.20	0.07	0.05	3.02	98.21	0.72	0.54	11	86
MB P-25	83.00	3.47	2.19	0.29	0.61	0.03	0.73	0.09	0.03	0.03	2.20	93.28			9	64
MB P-16	60.87	19.13	5.87	0.60	3.14	0.60	2.68	1.02	0.09	0.07	6.79	100.87	0.94	0.45	38	83
BT PO 28	84.47	6.02	2.79	0.66	1.40	0.15	1.08	0.62	0.08	0.03	1.57	100.28			16	60
BT PO 29	92.10	3.78	0.82	0.14	1.02	0.21	0.76	0.11	0.02	0.03	1.57	101.58			11	56
PO 1	75.34	8.04	7.37	1.04	0.55	0.03	1.06	0.52	0.07	0.18	4.30	98.50	0.74	0.58	14	87
PO 2-1	79.79	9.72	3.36	0.62	0.05	0.10	1.45	0.56	0.04	0.01	2.55	98.30			15	84
PO 3	88.09	7.16	1.74	0.15	–	–	0.75	0.53	0.02	0.00	1.62	100.06			7	90
PO 4-2	74.77	9.96	6.38	0.42	0.92	0.40	1.23	0.58	0.09	0.15	3.67	98.56	0.30	0.16	18	83
PO 4-4	67.92	6.79	9.36	0.87	4.40	0.34	1.43	0.40	0.07	0.28	6.74	98.59	1.31	1.21	29	76
PO 5	37.88	3.92	4.89	0.45	27.10	0.03	0.49	0.19	0.07	0.09	23.38	98.49	6.04	5.92	75	87
PO 6	45.19	2.17	1.41	0.34	26.81	0.02	0.16	0.11	0.14	0.12	21.91	98.38	5.86	5.76	71	91
PO 9	54.00	3.36	2.81	0.39	19.65	0.12	0.34	0.16	0.16	0.17	16.83	97.99	4.42	4.33	55	86
PO 11	84.53	6.15	3.20	0.18	0.34	0.05	0.93	0.46	0.09	0.03	2.04	98.35			10	78
BT PO 4	71.88	6.79	4.90	1.22	4.29	0.25	1.19	0.37	0.08	0.08	6.91	97.97	1.80	1.59	27	80
BT PO 5	68.46	6.44	5.28	1.15	6.87	0.08	0.94	0.35	0.08	0.08	9.26	98.99	2.40	2.24	29	85
BT PO 16	72.33	7.15	8.37	1.27	2.11	0.21	1.04	0.46	0.20	0.13	7.16	100.44	1.83	1.22	20	83
BT PO 30/2	68.44	12.29	5.23	1.17	2.68	0.31	1.72	0.70	0.09	0.06	5.60	98.30	1.21	0.75	28	84
FC 1	73.68	2.87	7.31	0.50	6.40	0.15	0.55	0.21	0.14	0.24	7.90	99.98	1.92	1.81	24	77
FC 2	77.89	3.83	10.22	0.80	0.40	0.15	0.53	0.24	0.09	0.21	5.60	99.97			9	71
FC 3	87.51	4.35	4.40	0.43	0.07	0.20	0.54	0.33	0.07	0.06	2.20	100.18			8	81
FC 5	74.16	6.86	11.27	0.57	0.13	0.40	1.20	0.50	0.14	0.23	4.60	100.10			16	76
CRM 1A	85.36	6.00	3.72	0.28	0.38	0.04	1.21	0.41	0.10	0.05	2.10	99.67			12	74
CRM 2	84.48	4.90	3.58	0.30	1.78	0.05	1.03	0.34	0.08	0.06	3.10	99.72			15	52
CRM 3	84.32	6.80	3.88	0.17	0.11	0.40	1.05	0.41	0.11	0.06	2.40	99.74			13	77
CM 1A	79.37	3.11	9.94	0.86	0.64	0.11	0.36	0.21	0.06	0.20	5.00	99.87			8	64
CM 3A	84.89	3.25	6.37	0.60	0.22	0.12	0.36	0.25	0.04	0.16	3.60	99.87			6	77
CM 3B	90.78	3.82	2.13	0.32	0.04	0.22	0.47	0.25	0.03	0.01	2.00	100.08			7	80
CM 4A	89.18	4.10	3.27	0.44	0.04	0.23	0.51	0.30	0.05	0.01	1.40	99.55			8	80
CM 4A_2	89.09	4.16	3.43	0.45	0.05	0.23	0.51	0.31	0.06	0.01	1.40	99.71			8	80
CM 5A	76.72	5.54	9.19	1.02	0.34	0.36	0.81	0.61	0.08	0.33	4.80	99.82			14	73
VN 1	79.31	10.69	3.19	0.82	0.06	0.51	1.65	0.65	0.08	0.02	2.50	99.52			21	80
VN 2	79.70	10.79	2.82	0.81	0.06	0.52	1.76	0.66	0.10	0.01	2.50	99.77			22	79
VN 3A	81.63	9.43	2.84	0.79	0.07	0.55	1.50	0.59	0.09	0.02	2.10	99.64			20	78
VN 3B	82.34	8.93	2.78	0.75	0.06	0.52	1.50	0.55	0.10	0.01	2.30	99.87			20	78
VN 4	79.00	11.45	2.83	0.82	0.04	0.48	2.00	0.66	0.07	0.01	2.60	100.00			24	79
VN 5	81.63	9.40	2.62	0.75	0.11	0.42	1.44	0.81	0.14	0.01	2.40	99.77			18	79

*Formations, late Devonian–Carboniferous, of the Cantabrian Mountains, northern Spain: Vergaño, VN; Vañes, CM; Carmen, FC, CRM; Potes Group, PO, BT PO; Murcia, BT, MB. Major elements were determined by ICP-ES after a $LiBO_2$ fusion at ACME Analytical Labs, Vancouver, Canada.

†CIA has been calculated according to Nesbitt and Young (1982) and Fedo *et al.* (1995). Ca in phosphates has not been considered in the calculation of the CIA, because CIA values increase by only *c.*1 unit if all P_2O_5 is assigned to apatite.

‡Calculation of CaO* is based on values of TC (total carbon) and TIC (total inorganic carbon) obtained by analysis using CS-Mat 5500, in the Department of Geology and Paleontology, Münster University. Only samples with increased values of CaO were selected. Those with low values did not show a reaction with HCl (10%); dolomite was not observed in thin section. CaO was consequently considered to be equal to CaO*.

–, below detection limit; blank spaces, not measured.

& Nesbitt 1999). Within this unit, rocks of diamictite facies commonly have the lowest CIA values (between 50 and 70). Diamictites in general represent either lodgement tills or moraine material that was rapidly redeposited by mass wasting in glaciomarine environments (e.g. Scheffler *et al.* 2003; Dobrzinski *et al.* 2004; Young *et al.* 2004; Rieu *et al.* 2007; Fig. 6.4). Such deposits with low CIA values are frequently associated with finer-grained and laminated glaciomarine sandstones, siltstones and shales, which may include ice-rafted debris, with higher CIA values between 70 and 85 (Fig. 6.4; Panahi & Young 1997; Dobrzinski *et al.* 2004; Young *et al.* 2004; Rieu *et al.* 2007).

Lower CIA values in glaciomarine deposits can be caused by several factors acting alone or in concert. K-metasomatism in connection with the conversion of illite to K-feldspar, or the illitization of kaolinite, is the most commonly cited cause (Nesbitt & Young 1989; Fedo *et al.* 1995). However, the grain-size of the analysed rock is also an important factor. Sands formed from chemically pre-weathered rocks and soils generally have lower CIA values and plot lower in the A–CN–K triangle than associated muds, because feldspars and other labile minerals tend to be concentrated in the coarser-grained fraction (Nesbitt *et al.* 1996; Fig. 6.3). Furthermore, sorting or mixing of known and cryptic sources may result in an unexpected change of the amount of feldspar in a deposit.

A sedimentary enrichment of K-feldspar relative to the assumed source rock causes the distribution of data in the A–CN–K diagram to mimic a K-metasomatic effect. In such a case the predicted weathering trend would shift to the right and point more closely to a muscovite rather than an illite composition on the A–K join of the diagram, or a CIA of 80 instead of 90 (Fig. 6.4; Nesbitt *et al.* 1997). A correction of the CIA data for an alleged K-metasomatism according to Fedo *et al.* (1995; Figs 6.3 and 6.4) would in this case lead to an overadjustment. A cause of increased or high CIA values in glaciomarine rocks may also be

Table 6.3. *CIA and WIP values of the Neoproterozoic Port Askaig Formation, Scotland, based on the data of Panahi & Young (1997) and our own analyses*

Sample	TC	TIC	WIP	CIA*	CIA_{corr} †
94-102	0.58	0.45	33	68	84
94-106	0.68	0.44	56	65	73
94-108	0.90	0.62	61	64	72
94-78	4.14	3.39	75	74	83
94-79	4.52	4.17	72	74	86
94-87	1.95	1.23	57	63	72
94-97	0.56	0.45	36	64	71
95-62	3.39	2.85	69	77	87
95-66	5.80	5.00	84	74	87
95-67	5.11	4.75	75	72	87
95-69	3.37	2.91	75	70	86
95-70	3.92	3.37	70	68	78
95-71	6.19	4.90	85	71	87
95-73	4.93	4.04	79	71	84
95-76	5.21	4.25	78	75	83
95-79	3.57	2.93	64	73	87
95-80	5.03	4.66	80	70	81
95-83	1.69	1.32	53	66	74
95-84	1.56	0.51	56	61	66

*Ca in phosphates has not been considered in the calculation of the CIA, because CIA values increase by only *c.*1 unit if all P_2O_5 is assigned to apatite. CIA has been calculated according to Nesbitt & Young (1982) and Fedo *et al.* (1995).

†CIA_{corr}: CIA value corrected to the predicted weathering trend according to Fedo *et al.* (1995).

Calculation of CaO* is based on values of TC (total carbon) and TIC (total inorganic carbon) obtained by analysis using CS-Mat 5500, in the Department of Geology and Paleontology, Münster University.

the incorporation of older, strongly weathered material into the glacial deposits (Nesbitt & Young 1997; Dobrzinski *et al.* 2004; Fig. 6.2).

Many Neoproterozoic glaciomarine successions are characterized by a deviation of the observed weathering trend from the predicted one and towards the K apex (Figs 6.3 and 6.4), including the lower and upper diamictites of the Yangtze platform in South China (Table 6.1; Dobrzinski *et al.* 2004), the Port Askaig Formation (Nesbitt & Young 1997; Tables 6.1 and 6.3), the Ghaub Formation of northern Namibia, the Norwegian Smalfjord and Mortensnes formations (Tables 6.1 and 6.4), and the Fiq Formation in Oman (Rieu *et al.* 2007). The same effect is also evident in the glacial Ordovician Table Mountain Group in South Africa (Young *et al.* 2004).

Regarding the Port Askaig and Fiq formations, the Chinese diamictites and the Table Mountain Group, K-metasomatism has in fact been cited as the cause of the deviation from the commonly used predicted weathering trend (Nesbitt & Young 1997; Dobrzinski *et al.* 2004; Young *et al.* 2004; Rieu *et al.* 2007). However, almost all the mentioned cases include analyses of matrix material of glaciomarine diamictites and associated coarse-grained strata. Some of the Neoproterozoic diamictites, including the ones from South China (Dobrzinski & Bahlburg 2007), have an impure shaley matrix rich in silt or fine sand. The presence of this coarser material in the matrix of the diamictites may have contributed consequently to a deviation of the observed weathering trends from the predicted one.

A combination of grain-size effects and the variable incorporation of older weathered material into the Neoproterozoic glaciomarine deposits may account for the measured CIA values (Fig. 6.4; Tables 6.2 to 6.4). In view of the corrected CIA values

Table 6.4. *Major element whole-rock compositions and weathering indices*

Sample*†	SiO_2	Al_2O_3	Fe_2O_3	MgO	CaO¶	Na_2O	K_2O	TiO_2	P_2O_5	MnO	LOI	Total	TC	TIC	WIP	CIA§	CIA_{corr}‖
GF 1	70.77	6.66	15.52	0.4	0.05	0.05	3.17	1.24	0.12	0.01	1.50	99.50	0.03	–‡	29	65	87
GF 2	81.78	8.45	2.31	0.42	0.01	0.1	5.22	0.43	0.06	0.01	1.20	99.98	0.01	–	46	59	87
GF 3	72.25	7.50	10.25	0.95	0.47	0.09	4.79	0.34	0.35	0.04	2.70	99.73	0.06	0.01	45	55	79
GF 4	28.42	6.46	2.82	10.93	19.89	0.86	2.14	0.40	0.12	0.06	27.80	99.91	7.48	7.26	107	63	72
GF 5	38.51	7.33	3.44	9.29	15.52	0.83	2.55	0.43	0.14	0.06	21.70	99.80	5.66	5.34	94	64	74
GF 7	27.84	4.28	3.20	12.98	19.08	0.22	1.79	0.24	0.10	0.08	30.00	99.82	7.91	7.65	102	65	81
GF 8	59.81	16.53	7.32	3.15	0.70	0.74	5.36	0.87	0.18	0.11	5.00	99.80	0.23	0.09	63	69	80
GF 9	33.92	7.96	4.97	10.47	15.03	0.91	2.82	0.47	0.14	0.14	23.00	99.83	6.09	5.62	99	64	74
GF 11	71.33	13.72	3.68	1.11	0.56	2.20	4.93	0.44	0.14	0.03	1.70	99.84	0.07	0.06	67	59	68
GF 12	73.82	12.63	3.39	0.96	0.31	2.06	4.49	0.42	0.12	0.05	1.60	99.86	0.03	0.02	61	59	68
GF 13	7.93	0.84	0.48	19.65	27.73	0.02	0.29	0.06	0.07	0.60	42.30	99.98	11.13	10.92	127	71	85
S1	73.68	10.67	3.59	1.89	1.42	1.45	2.82	0.5	0.12	0.03	3.20	99.38	0.36	0.27	46	65	70
S2	73.22	11.95	4.10	1.72	0.41	1.03	3.66	0.65	0.11	0.02	2.50	99.38	0.08	–	46	65	73
S3	67.36	13.36	5.94	2.94	0.27	1.41	3.91	0.83	0.17	0.10	3.10	99.40	0.09	0.04	55	67	74
S4	59.38	11.26	4.65	4.85	4.74	1.37	3.48	0.79	0.16	0.06	8.80	99.55	1.88	1.56	68	65	73
S5	69.49	12.75	3.91	2.33	1.48	1.91	3.39	0.61	0.11	0.03	3.40	99.42	0.46	0.32	57	65	70
S6	65.02	14.83	5.73	2.6	1.05	1.86	4.00	0.70	0.13	0.04	3.50	99.48	0.24	0.17	61	65	69
M1	64.35	15.52	6.23	3.13	0.33	2.05	3.58	0.78	0.14	0.05	3.30	99.48	0.06	0.06	59	68	72
M2	64.14	15.93	5.49	2.67	0.89	2.36	3.76	0.82	0.15	0.04	3.20	99.46	0.16	0.14	63	65	69
M3	69.19	10.5	3.88	3.05	2.98	1.45	2.45	0.51	0.11	0.05	5.20	99.38	0.95	0.73	50	68	73
M4	67.96	11.91	4.44	2.88	2.35	1.96	2.42	0.58	0.12	0.06	4.70	99.40	0.78	0.56	53	67	69
M5	65.56	11.05	5.19	3.01	3.43	1.85	2.13	0.54	0.10	0.10	6.20	99.17	1.11	0.79	52	67	69
M6	63.64	14.2	5.79	3.39	2.00	2.45	2.61	0.69	0.13	0.10	4.40	99.43	0.46	0.29	59	64	64

*Neoproterozoic Ghaub Formation (GF), northern Namibia, and the Smalfjord (S) and Mortensnes (M) formations, northern Norway. Samples of the Ghaub Formation diamictites were taken on the Ghaub and Jakkalumuramba farms NE of the town of Otavi. Analyses represent matrix compositions.

†Major elements were determined by ICP-ES after a $LiBO_2$ fusion at ACME Analytical Labs, Vancouver, Canada.

–below detection limit.

§CIA has been calculated according to Nesbitt & Young (1982) and Fedo *et al.* (1995). Ca in phosphates has not been considered in the calculation of the CIA, because CIA values increase by only *c.*1 unit if all P_2O_5 is assigned to apatite.

‖CIA_{corr}: CIA value corrected to the predicted weathering trend according to Fedo *et al.* (1995).

¶Calculation of CaO* is based on values of TC (total carbon) and TIC (total inorganic carbon) obtained by analysis using CS-Mat 5500, in the Department of Geology and Paleontology, Münster University.

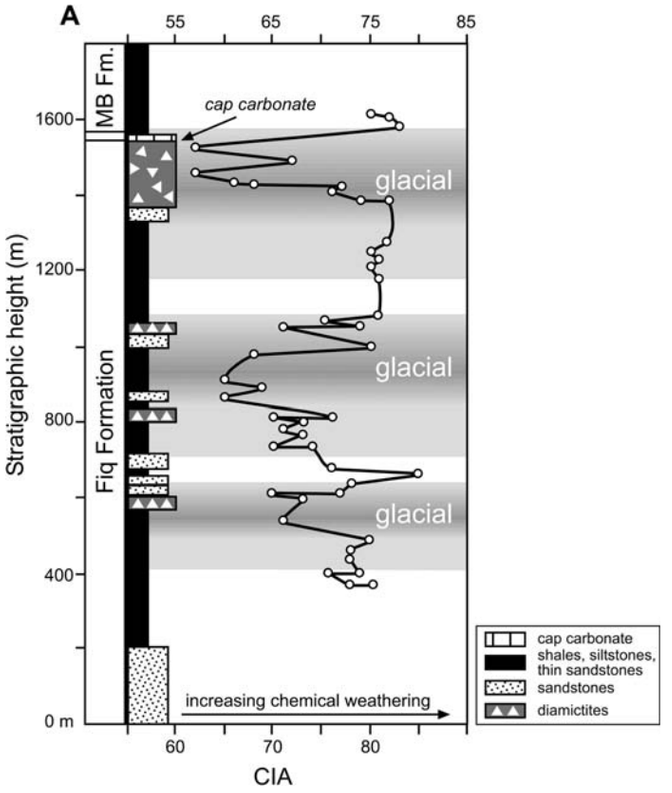

Fig. 6.6. Variations in the CIA with stratigraphic height in the Fiq Formation, Oman. MB Fm., Masirah Bay Formation. Modified from Rieu *et al.* (2007).

shown in Figure 6.4 and the discussion in the preceding paragraphs, we conclude that in particular the high values are overcorrected maximum values very likely exaggerating the magnitude of changes due to chemical weathering.

Implications for the study of Neoproterozoic climate change

The origin of Neoproterozoic diamictite successions was debated long before the 'Snowball Earth' hypothesis was proposed (Kirschvink 1992; Hoffman *et al.* 1998; Hoffman & Schrag 2002). Classic examples like the Ghaub diamictites in northern Namibia were repeatedly interpreted either as tillites and glaciomarine sediments (e.g. Gevers 1931; Martin 1964; Hoffmann & Prave 1996; Hoffman & Schrag 2002) or as tectonically triggered mass flow deposits (e.g. Schermerhorn 1974; Martin *et al.* 1985; Eyles & Januszczak 2007). Furthermore, there are also cases where alleged glacial deposits were proven to be in fact of depositional origin unrelated to ice action and cold climates. Examples include purported tillites of Tremadoc age in the Andes of northwestern Argentina (Keidel 1943), which were demonstrated to be coastal conglomerates (Bahlburg 1990), and conglomeratic deposits in northern Chile allegedly linked to the Late Palaeozoic Gondwana glaciation (Cecioni 1979, 1981), which were shown to be of mass-flow origin in turbidite complexes (Charrier 1986; Bahlburg & Breitkreuz 1993).

It is usually necessary to support one line of evidence with at least a second, independent one in order to have confidence that an interpretation is correct. This applies not only to controversial sedimentological cases. The analysis of the CIA is a powerful tool in studies of the palaeoclimatic record preserved in siliciclastic sedimentary successions. However, as discussed previously, numerous factors can influence the major element geochemical composition of a siliciclastic rock. Thus, CIA values alone are almost meaningless as climate indicators when not considered in the context of the stratigraphic framework and facies of the analysed sedimentary rock. This is demonstrated very well in a study of the Fiq Formation in Oman (Rieu *et al.* 2007; Fig. 6.6), an association of alternating glacial diamictites, debris-flow deposits, turbidite sandstones, hemipelagic shales, and wave-rippled shoreface deposits. The facies changes are connected to coincident changes between low CIA values of 62–70 for the glacial diamictite matrix, and high ones between 80 and 85 (corrected after Fedo *et al.* 1995) for shales, siltstones and fine-grained sandstones. Facies changes and CIA data give evidence of variations in the intensity of chemical weathering as a function of climate oscillations between glacial and warm–humid interglacial conditions (Rieu *et al.* 2007). Scheffler *et al.* (2003) presented similar data in a study of the waning phase of the Late Palaeozoic glaciation in South Africa recorded in the Dwyka Group. In the Neoproterozoic as well as in the Late Palaeozoic, these climate oscillations together with the facies of the respective deposits give evidence of a functioning hydrological cycle and sediment dispersal systems. In the Neoproterozoic case these data are in direct opposition to assumptions of a totally ice-covered Snowball Earth as proposed by Hoffman & Schrag (2002).

These CIA values are compatible with a prominent influence of physical weathering on the production of the diamictite detrital silicate matrix. Together with sedimentological features including the presence of dropstones in laminated facies, these values strengthen interpretations of a glacially connected origin of the Ghaub diamictites.

The interpretation of the Neoproterozoic Smalfjord and Mortensnes formations of northern Norway is less controversial and centres around the question whether the strata represent redeposited detritus originally produced in a glacial environment (Arnaud & Eyles 2002) or deposits of direct glacial action (Edwards 2004; Rice 2004). Application of the CIA cannot solve these differences in a fundamentally sedimentological controversy. The uncorrected CIA values of the Smalfjord and Mortensnes formations (Table 6.4) are uniformly low between 65 and 68, and between 64 and 74 (averages of 72 and 69, respectively) if corrected according to Fedo *et al.* (1995; Fig. 6.4). It is thus legitimate to infer at least a glacial origin for the detritus.

The Neoproterozoic lower and upper glacial diamictites of the Yangtze platform represent associations of lodgement till, subglacial melt-out deposits of grounded glaciers, sediments of concentrated density flows and glacial outwash, and turbidites and laminated deposits containing ice-rafted debris (Dobrzinski & Bahlburg, 2007). CIA values of both diamictite units are between 50 and 90 (Fig. 6.4; Table 6.1; Dobrzinski *et al.* 2004). Correction of values following Fedo *et al.* (1995) does not change their range but leads to a shuffling of values within this range. The corrected average value is 72 (Fig. 6.4). The combination of low values in the matrix of glacial diamictites and higher values in associated glacial facies is interpreted as a result of reworking of older, weathered material into the glacial deposits (Dobrzinski *et al.* 2004). This is evident in some sections showing a decrease in CIA values upsection (Fig. 6.2).

The non-glacial units of the China platform consisting of preglacial siliciclastics, the shales and carbonates of the Datangpo Formation intercalated between the glacial units, and the postglacial carbonates and shales of the Doushantuo Formation (Table 6.1) have CIA values ranging between 59 and 97 with abundant higher values. The corrected ranges are rather similar, with a corrected average of 76 (Fig. 6.4). The higher values of the non-glacial deposits relative to the diamictite successions are taken to reflect more humid and warmer weathering and climate conditions. Particularly noteworthy is the presence of K-feldspar and plagioclase in the silicate fraction contained in the Marinoan cap carbonates in South China indicating the minor influence of chemical weathering on the silicate detritus in these strata (Dobrzinski 2005).

Conclusions

The CIA (Nesbitt & Young 1982) is the most widely applied and most indicative of the available weathering indices. When the intricacies of the weathering systems and of applying the index are appropriately considered (Fedo *et al.* 1995; Nesbitt & Young 1996; Nesbitt *et al.* 1997; Young 2001; and discussion of Fig. 6.4), the index is a very valuable tool in the assessment of past climate change as recorded by siliciclastic sedimentary rocks, with one critical caveat: it needs to be applied in conjunction with a comprehensive facies analysis. Concerning the Neoproterozoic glacial periods, the combination of both data sets gives strong evidence of (i) a functioning hydrological cycle, (ii) operative sediment routing systems, and (iii) variable climate conditions oscillating between dry–cool and glacial, and warm–humid and interglacial. These findings are incompatible with the hypothesis of a totally ice-covered Snowball Earth.

H. Rice (Vienna, Austria) kindly supplied samples of the Smalfjord and Mortensnes formations of northern Norway. We thank G. Young (London, Ontario, Canada) for sending us sample powders of the Panahi & Young (1997) samples of the Port Askaig Formation. This study was supported by the German Research Foundation DFG (grants Ba 1011/23-1,2,3). This paper is a contribution to IGCP project 512 'Neoproterozoic Ice Ages'. We thank A.R. Prave (St. Andrews, Scotland), C. Augustsson and C. Reimann (Münster, Germany), for commenting on earlier versions of the manuscript. We appreciate the very constructive reviews by Hilmar v. Eynatten (Göttingen, Germany) and an anonymous reviewer. B. Fister (Münster) kindly re-drafted Figure 6.6.

References

Aristizábal, E., Roser, B. & Yokota, S. 2005. Tropical chemical weathering of hillslope deposits and bedrock source in the Aburrá Valley, northern Colombian Andes. *Engineering Geology*, **81**, 389–406.

Arnaud, E. & Eyles, C. 2002. Glacial influence on Neoproterozoic sedimentation: the Smalfjord Formation, northern Norway. *Sedimentology*, **49**, 765–788.

Arnaud, E. & Eyles, C. 2006. Neoproterozoic environmental change recorded in the Port Askaig Formation, Scotland: climatic vs tectonic controls. *Sedimentary Geology*, **183**, 99–124.

Arnaud, E. & Fairchild, I. J. 2011. The Port Askaig Formation, Dalradian Supergroup, Scotland. *In*: Arnaud, E., Halverson, G. P. & Shields-Zhou, G. (eds) *The Geological Record of Neoproterozoic Glaciations*. Geological Society, London, Memoirs, **36**, 635–642.

Bahlburg, H. 1990. The Ordovician basin in the Puna of NW Argentina and N Chile: geodynamic evolution from back-arc to foreland basin. *Geotektonische Forschungen*, **75**, 1–107.

Bahlburg, H. 1998. The geochemistry and provenance of Ordovician turbidites in the Argentinian Puna. *In*: Pankhurst, R. J. & Rapela, C. W. (eds) *The Proto-Andean Margin of Gondwana.* Geological Society, London, Special Publication, **142**, 127–142.

Bahlburg, H. & Breitkreuz, C. 1993. Differential response of a Devonian–Carboniferous platform-deeper basin system to sea-level change and tectonics, N. Chilean Andes. *Basin Research*, **5**, 21–40.

Baum, S. K. & Crowley, T. J. 2003. The snow/ice instability as a mechanism for rapid climate change: a Neoproterozoic snowball Earth model example. *Geophysical Research Letters*, **30**, 2030, doi: 10.1029/2003GL017333.

Benn, D. I. & Prave, A. R. 2006. Subglacial and proglacial glacitectonic deformation in the Neoproterozoic Port Askaig Formation, Scotland. *Geomorphology*, **75**, 266–280.

Bhatia, M. R. & Crook, K. A. W. 1986. Trace element characteristics of graywackes and tectonic setting discrimination of sedimentary basins. *Contributions to Mineralogy and Petrology*, **92**, 181–193.

Bland, W. & Rolls, D. 1998. *Weathering. An Introduction to the Scientific Principles*. Arnold Publishers, London.

Cecioni, G. 1979. Grupo El Toco, desierto de Atacama, Chile. *Revista de la Asociación Geológica Argentina*, **34**, 211–223.

Cecioni, G. , 1981. Triassic El Toco Group, Atacama Desert, Chile. *In*: Hambrey, M. J. & Harland, W. B. (eds) *Earth's Pre-Pleistocene Glacial Record*. Cambridge University Press, Cambridge.

Charrier, R. 1986. The Gondwana glaciation in Chile: description of alleged glacial deposits and paleogeographic conditions bearing on the extension of the ice cover in Southern South America. *Palaeogeography, Palaeoclimatology, Palaeoecology*, **56**, 151–175.

Condie, K. C. 1993. Chemical composition and evolution of the upper continental crust: contrasting results from surface samples and shales. *Chemical Geology*, **104**, 1–37.

Condie, K. C., Des Marais, D. J. & Abbott, D. 2001. Precambrian superplumes and supercontinents: a record in black shales, carbon isotopes, and paleoclimates? *Precambrian Research* **106**, 239–260.

Crowell, J. C. 1999. Pre-Mesozoic ice ages: their bearing on understanding the climate system. *Geological Society of America Memoir*, **192**, 1–106.

Crowley, T. J. & North, G. R. 1991. Paleoclimatology. *Oxford Monographs on Geology and Geophysics*, **18**, 349.

Dobrzinski, N. 2005. *Das Paradoxon äquatornah abgelagerter glazialer Sedimentfolgen: Sedimentologische und geochemische Klimaindizien von der neoproterozoischen Yangtze Plattform (Südchina)*. Dissertation, Westfälische Wilhelms-Universität, Münster, Germany.

Dobrzinski, N. & Bahlburg, H. 2007. Sedimentology and environmental significance of the Cryogenian successions of the Yangtze platform, South China block. *Palaeogeography, Palaeoclimatology, Palaeoecology*, **254**, 100–122.

Dobrzinski, N., Bahlburg, H., Strauss, H. & Zhang, Q. R. 2004. Geochemical climate proxies applied to the Neoproterozoic glacial succession on the Yangtze Platform, South China. *In*: Jenkins, G., McMenamin, M., McKay, C. P. & Sohl, L. (eds) *The Extreme Proterozoic: Geology, Geochemistry and Climate*. American Geophysical Union Monograph Series, **146**, 13–32.

Duzgoren-Aydin, N. S., Aydin, A. & Malpas, J. 2002. Re-assessment of chemical weathering indices: case study of pyroclastic rocks of Hong Kong. *Engineering Geology*, **63**, 99–119.

Edwards, M. B. 2004. Glacial influence on Neoproterozoic sedimentation: the Smalfjord Formation, northern Norway — discussion. *Sedimentology*, **51**, 1409–1417.

Etienne, J. L., Allen, P. A., Rieu, R. & Le Gerroué, E. 2008. *Neoproterozoic glaciated basins: a critical review of the Snowball Earth hypothesis by comparison with Phanerozoic glaciations*. Special Publication of the International Association of Sedimentologists Special Publication 39.

Evans, D. A. D. 2000. Stratigraphic, geochronological, and paleomagnetic constraints upon the Neoproterozoic climatic paradox. *American Journal of Science*, **300**, 347–433.

Eyles, N. 2008. Glacio-epochs and the supercontinent cycle after ~3.0 Ga: Tectonic boundary conditions for glaciation. *Palaeogeography, Palaeoclimatology, Palaeoecology*, **258**, 89–125.

Eyles, N. & Januszczak, N. 2007. Syntectonic subaqueousmass flows of the Neoproterozoic Otavi Group, Namibia: where is the evidence of global glaciation? *Basin Research*, **19**, 179–198.

Fairchild, I. J. & Kennedy, M. J. 2007. Neoproterozoic glaciation in the Earth system. *Journal of the Geological Society, London*, **164**, 895–921.

Fedo, C. M., Nesbitt, H. W. & Young, G. M. 1995. Unraveling the effects of potassium metasomatism in sedimentary rocks and paleosols, with implications for paleoweathering conditions and provenance. *Geology*, **23**, 921–924.

Gallet, S., Jahn, B., Van Vliet Lano, B., Dia, A. & Rosello, E. 1998. Loess geochemistry and its implications for particle origin and composition of the upper continental crust. *Earth and Planetary Science Letters*, **156**, 157–177.

Gevers, T. W. 1931. An ancient tillite in South West Africa. *Transactions of the Geological Society of South Africa*, **34**, 1–17.

Gutzmer, J. & Beukes, N. J. 1998. Earliest laterites and possible evidence for terrestrial vegetation in the Early Proterozoic. *Geology*, **26**, 263–266.

Hoffman, P. F. 2011. Glaciogenic and associated strata of the Otavi carbonate platform and foreslope, northern Namibia: evidence for large base-level and glacioeustatic changes. *In*: Arnaud, E., Halverson, G. P. & Shields-Zhou, G. (eds) *The Geological Record of the Neoproterozoic Glaciations*. Geological Society, London, Memoirs, **36**, 195–209.

Hoffman, P. F. & Schrag, D. P. 2002. The snowball Earth hypothesis: testing the limits of global change. *Terra Nova*, **14**, 129–155.

Hoffman, P. F., Kaufman, A. J., Halverson, G. P. & Schrag, D. P. 1998. A Neoproterozoic snowball Earth. *Science*, **281**, 1342–1346.

Hoffmann, K. H. & Prave, A. R. 1996. A preliminary note on a revised subdivision and regional correlation of the Otavi group based on glacigenic diamictites and associated cap dolostones. *Communications of the Geological Survey of Namibia*, **11**, 81–86.

IGME 1984. Mapa Geológica de España a escala 1:50.000, Hoja no. 107 (Barruelo de Santullan), 113.

ITGE 1994. Mapa Geológica de España a escala 1:50.000, Hoja no. 81 (Potes), 128.

Johnsson, M. J. 1993. The system controlling the composition of clastic sediments. *In*: Johnsson, M. J. & Basu, A. (eds) *Processes Controlling the Composition of Clastic Sediments.* Geological Society of America Special Paper, **285**, 1–19.

Johnsson, M. J., Stallard, R. F. & Meade, R. H. 1988. First-cycle quartz arenites in the Orinoco River Basin, Venezuela and Colombia. *Journal of Geology*, **96**, 263–277.

Kahmann, J. A., Seaman, J. III & Driese, S. G. 2008. Evaluating trace elements as paleoclimate indicators: multivariate statistical analysis of Late Mississippian Pennington Formation paleosols, Kentucky, U.S.A. *Journal of Geology*, **116**, 254–268.

Keidel, J. 1943. El Ordovícico inferior en los Andes del norte Argentino y sus depósitos marino glaciales. *Boletin de la Academía Nacional de Ciencias de Córdoba*, **36**, 140–229.

Keller, M., Bahlburg, H. & Reuther, C.-D. 2008. The transition from passive to active margin sedimentation in the Cantabrian Mountains, Northern Spain: Devonian or Carboniferous? *Tectonophysics*, doi: 10.1016/j.tecto.2008.06.022

Keller, M., Bahlburg, H., Reuther, C.-D. & Weh, A. 2007. Flexural to broken foreland basin evolution as a result of Variscan collisional events in northwestern Spain. *In*: Hatcher, R. D. Jr, Carlson, M. P., McBride, J. H. & Martínez Catalán, J. R. (eds) *The 4D Framework of Continental Crust.* Geological Society of America Memoir, **200**, 489–510.

Kirschvink, J. L. 1992. Late Proterozoic low-latitude global glaciation: the snowball earth. *In*: Schopf, J. W & Klein, C. (eds) *The Proterozoic Biosphere*. Cambridge University Press, Cambridge, 51–52.

Kramer, J. R. 1968. Mineral-water equilibria in silicate weathering. *International Geological Congress, 23rd session, Section 6*, 149–160.

Martin, H. 1964. Beobachtungen zum Problem der jung-präkambrischen glazialen Ablagerungen in Südwestafrika. *Geologische Rundschau*, **54**, 115–127.

Martin, H., Porada, H. & Walliser, O. H. 1985. Mixtite deposits of the Damara sequence, Namibia: problem of interpretation. *Palaeogeography, Palaeoclimatology, Palaeoecology*, **51**, 159–196.

McLennan, S. M. 1993. Weathering and global denudation. *Journal of Geology*, **101**, 295–303.

McLennan, S. M. 2001. Relationships between the trace element composition of sedimentary rocks and upper continental crust. *Geochemistry, Geophysics, Geosystems* (G^3), **2**, doi:10.1029/2000GC000109.

McLennan, S. M., Hemming, S., McDaniel, D. K. & Hanson, G. N. 1993. Geochemical approaches to sedimentation, provenance and tectonics. *In*: Johnsson, M. J. & Basu, A. (eds) *Processes Controlling the Composition of Clastic Sediments*. Geological Society of America Special Paper, **285**, 21–40.

Nedachi, Y., Nedachi, M., Bennett, G. & Ohmoto, H. 2005. Geochemistry and mineralogy of the 2.45 Ga Pronto paleosols, Ontario, Canada. *Chemical Geology*, **214**, 21–44.

Nesbitt, H. W. & Young, G. M. 1982. Early Proterozoic climates and plate motions inferred from major element chemistry of lutites. *Nature*, **199**, 715–717.

Nesbitt, H. W. & Young, G. M. 1984. Prediction of some weathering trends of plutonic and volcanic rocks based on thermodynamic and kinetic considerations. *Geochimica et Cosmochimica Acta*, **48**, 1523–1534.

Nesbitt, H. W. & Young, G. M. 1989. Formation and diagenesis of weathering profiles. *Journal of Geology*, **97**, 129–147.

Nesbitt, H. W. & Young, G. M. 1996. Petrogenesis of sediments in the absence of chemical weathering: effects of abrasion and sorting on bulk composition and mineralogy. *Sedimentology*, **42**, 341–358.

Nesbitt, H. W., Fedo, C. M. & Young, G. M. 1997. Quartz and feldspar stability, steady and non-steady-state weathering, and petrogenesis of siliciclastic sands and muds. *Journal of Geology*, **105**, 173–191.

Nesbitt, H. W., Young, G. M., McLennan, S. M. & Keays, R. R. 1996. Effects of chemical weathering and sorting on the petrogenesis of siliciclastic sediments, with implications for provenance studies. *Journal of Geology*, **104**, 525–542.

Ohta, T. & Arai, H. 2007. Statistical empirical index of chemical weathering in igneous rocks: a new tool for evaluating the degree of weathering. *Chemical Geology*, **240**, 280–297.

Panahi, A. & Young, G. M. 1997. A geochemical investigation into the provenance of the Neoproterozoic Port Askaig Tillite, Dalradian Supergroup, western Scotland. *Precambrian Research*, **85**, 81–96.

Parker, A. 1970. An index of weathering for silicate rocks. *Geological Magazine*, **107**, 501–504.

Pettijohn, F. J., Potter, P. E. & Siever, R. 1987. *Sand and Sandstone*. Springer, New York.

Rice, A. H. N. 2004. Glacial influence on Neoproterozoic sedimentation: the Smalfjord Formation, northern Norway – discussion. *Sedimentology*, **51**, 1419–1422.

Rice, A. H. N. & Hofmann, C. C. 2001. The transition from Neoproterozoic glacial to interglacial sedimentation near Hammarnes, East Finnmark, North Norway. *Norsk Geologisk Tidsskrift*, **81**, 257–262.

Rice, A. H. N., Edwards, M. B., Hansen, T. A., Arnaud, E. & Halverson, G. P. 2011. Glaciogenic rocks of the Neoproterozoic Smalfjord and Mortensnes Formations, Vestertana Group, E. Finnmark, Norway. *In*: Arnaud, E., Halverson, G. P. & Shields-Zhou, G. (eds) *The Geological Record of Neoproterozoic Glaciations*. Geological Society, London, Memoirs, **36**, 593–602.

Rieu, R., Allen, P. A., Plotze, M. & Pettke, T. 2007. Compositional and mineralogical variations in a Neoproterozoic glacially influenced succession, Mirbat area, south Oman: Implications for paleoweathering conditions. *Precambrian Research*, **154**, 248–265.

Ruxton, B. P. 1968. Measures of the degree of chemical weathering of rocks. *Journal of Geology* **76**, 518–527.

Scheffler, K., Hoernes, S. & Schwark, L. 2003. Global changes during Carboniferous–Permian glaciation of Gondwana: Linking polar and equatorial climate evolution by geochemical proxies. *Geology*, **31**, 605–608.

Schermerhorn, L. J. G. 1974. Late Precambrian mixtites: glacial and/or non-glacial? *American Journal of Science*, **274**, 673–824.

Schrag, D. P., Berner, R. A., Hoffman, P. F. & Halverson, G. P. 2002. On the initiation of Snowball Earth. *Geochemistry, Geophysics, Geosystems*, **3**, doi:10.1029/2001GC000219.

Shields, G. A. 2008. Palaeoclimate – Marinoan meltdown. *Nature Geoscience*, **1**, 351–353.

Taylor, S. R. & McLennan, S. M. 1985. *The Continental Crust: Its Composition and Evolution*. Blackwell, Oxford.

von Eynatten, H. 2004. Statistical modelling of compositional trends in sediments. *Sedimentary Geology*, **171**, 79–89.

von Eynatten, H., Barceló-Vidal, C. & Pawlowsky-Glahn, V. 2003. Modelling compositional change: the example of chemical weathering of granitoid rocks. *Mathematical Geology*, **35**, 231–251.

Wagner, R. H. & Wagner-Gentis, C. H. T. 1963. Summary of the stratigraphy of Upper Paleozoic rocks in NE. Palencia, Spain. *Proceedings Kongelige Nederlandse Akademie Wetenschappen (B) LXVI*, **3**, 149–163.

Weil, A. B., Van der Voo, R. & Van der Pluijm, B. A. 2001. Oroclinal bending and evidence against the Pangea megashear; the Cantabria–Asturias Arc (northern Spain). *Geology*, **29**, 991–994.

Wintsch, R. P. & Kvale, C. M. 1994. Differential mobility of elements in burial diagenesis of siliciclastic rocks. *Journal of Sedimentary Research*, **A64**, 349–361.

Young, G. M. 2001. Comparative geochemistry of Pleistocene and Paleoproterozoic (Huronian) glaciogenic laminated deposits: relevance to crustal and atmospheric composition in the last 2.3 Ga. *Journal of Geology*, **109**, 463–477.

YOUNG, G. M. & NESBITT, H. W. 1999. Paleoclimatology and provenance of the glaciogenic Gowganda Formation (Paleoproterozoic), Ontario, Canada: a chemostratigraphic approach. *Geological Society of America Bulletin*, **111**, 264–274.

YOUNG, G. M., MINTER, W. E. L. & THERON, J. N. 2004. Geochemistry and palaeogeography of upper Ordovician glaciogenic sedimentary rocks in the Table Mountain Group, South Africa. *Palaeogeography, Palaeoclimatology, Palaeoecology*, **214**, 323–345.

ZHANG, Q.-R., CHU, X.-L. & FENG, L.-J. 2011. Neoproterozoic glacial records in the Yangtze Region, China. *In*: ARNAUD, E., HALVERSON, G. P. & SHIELDS-ZHOU, G. (eds) *The Geological Record of Neoproterozoic Glaciations*. Geological Society, London, Memoirs, **36**, 357–366.